Physics Letters A 384 (2020) 126754

Contents lists available at ScienceDirect

Physics Letters A

www.elsevier.com/locate/pla

Theoretical study of enhanced ferromagnetism and tunable magnetic anisotropy of monolayer CrI_3 by surface adsorption

Qin-Fang Xu [a,b], Wen-Qiang Xie [b], Zhi-Wei Lu [b], Yu-Jun Zhao [b,*]

[a] Department of Basic Courses, Guangzhou Maritime University, Guangzhou 510725, China
[b] Department of Physics, South China University of Technology, Guangzhou 510640, China

ARTICLE INFO

Article history:
Received 27 March 2020
Received in revised form 23 June 2020
Accepted 21 July 2020
Available online 27 July 2020
Communicated by L. Ghivelder

Keywords:
Monolayer CrI_3
Magnetic anisotropy energy
Li adsorption
First-principles calculation

ABSTRACT

Magnetic anisotropy energy (MAE) plays a key role for 2D magnetic materials, which have attracted significant attention for their promising applications in spintronic devices. Based on first-principles calculations, we have investigated the influence of surface adsorption on the ferromagnetism and MAE of monolayer CrI_3. We find that Li adsorption can dramatically enhance its ferromagnetism, and tune its easy magnetization axis to the in-plane direction from original out-of-plane at certain coverage of Li. The monotonic enhancement of in-plane magnetism in CrI_3 as the coverage of Li increases are attributed to electrostatic doping induced by charge transfer between Li atoms and I atoms, as supported by the charge doping simulation. The tunable robust magnetic anisotropy may open new promising applications of CrI_3–based materials in spintronic devices.

1. Introduction

Two dimensional materials (2D) have attracted growing attention due to potential applications in various fields, such as electronic devices [1–4], optoelectronic devices [5], and catalysts [6]. However, the development of applications of 2D materials in spintronics was lagged in the pace, due to the lack of magnetic ordering in conventional 2D materials. Many efforts, both experimental and theoretical, have been conducted to extrinsically introduce magnetism into nonmagnetic 2D materials or to seek 2D materials with intrinsic magnetism. On the one hand, the general methods of inducing magnetism in nonmagnetic 2D materials were substitutional doping [7,8], defect engineering [9], magnetic proximity effect [10] and so on. Although some achievements have been made by these approaches, the introduced magnetism is relatively weak and difficult to control experimentally. On the other hand, a variety of theoretical prediction about new 2D ferromagnetic materials have been reported by using density functional theory (DFT) calculations [11–17], and monolayer CrI_3 was one of them [15]. Until very recently, a great experimental breakthrough was made in 2D ferromagnetic materials. Zhang's group discovered that 2D ferromagnetic ordering exists in bilayer $Cr_2Ge_2Te_6$ [18]. Xu's group demonstrated 2D ferromagnetism in exfoliated monolayer CrI_3 [19]. Then room-temperature ferromagnetism was reported in 2D monolayer VSe_2 [20], $MnSe_x$ [21], and Fe_3GeTe_2 [22], Fe_5GeTe_2 [23] subsequently. These findings provide new exciting opportunities for future spintronic applications.

Magnetic order in 2D materials is always coupled to magnetic anisotropy, which overcomes the thermal fluctuations and stabilizes the magnetic order at the finite temperature based on the Mermin–Wagner theorem [24]. Moreover, ferromagnetic 2D materials with large anisotropy will be critical for spintronic applications. It is considerably attractive to explore whether intrinsic ferromagnetism and the magnetic anisotropy of 2D monolayer can be modulated. Previous works indicated that surface adsorption is an attractive approach to control electronic structure and magnetism in 2D materials [25,26]. By adsorption, a charge transfer can be induced between adatoms and the neighbor atoms of host materials, leading to an electrostatic doping. As is well known, Li is a typical electron donor, likely transfers charge to the substrate when adsorbed. Such a doping effect can give rise to a gate-tuned room temperature ferromagnetism in 2D magnetic Fe_3GeTe_2 [22]. Moreover, Jiang et al. reported that the magnetic properties of monolayer CrI_3 can be controlled by electrostatic doping using CrI_3-graphene vertical heterostructures [27]. The magnetic anisotropy energy (MAE) largely increased by surface adsorption in monolayer $Cr_2Ge_2Te_6$ [26] from DFT calculations. In addition, it is found that the MAE of CrI_3 is related to temperature and thickness experimentally [28–30].

In this work, the impact of Li adsorption on monolayer CrI_3 on the electronic and magnetic properties is investigated by first-principles calculations. We find that the easy axis of monolayer

* Corresponding author.
E-mail address: zhaoyj@scut.edu.cn (Y.-J. Zhao).

https://doi.org/10.1016/j.physleta.2020.126754
0375-9601/

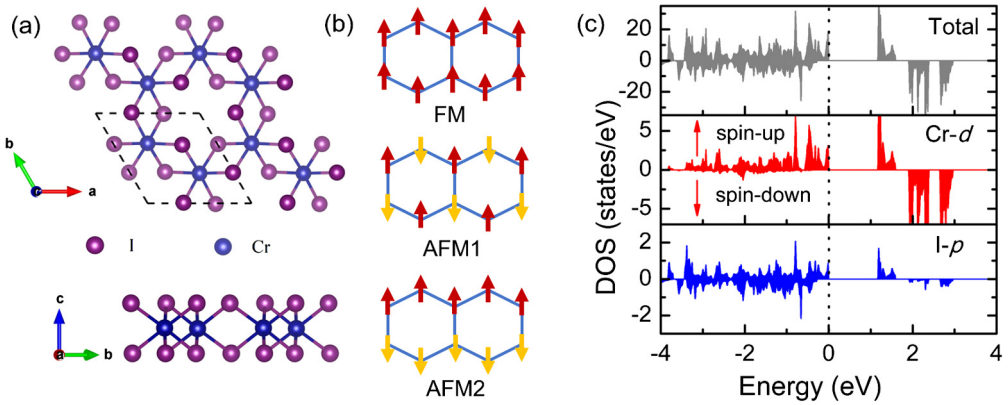

Fig. 1. (a) Top view and side view of crystalline structure of pristine monolayer CrI_3. The dashed rhombus represents the conventional unit cell. Blue and purple spheres represent Cr and I atoms, respectively. (b) The three possible magnetic configurations, namely, ferromagnetic (FM) state, antiferromagnetic (AFM) states. (c) Spin-resolved total and projected density of states for monolayer CrI_3. The valence band maximum is set to zero as marked with dot lines. (For interpretation of the colors in the figure(s), the reader is referred to the web version of this article.)

CrI_3 can be tuned from the out-of-plane to in-plane after Li adsorption, and the MAE reaches as large as 7 times greater than that of pristine CrI_3. When the monolayer CrI_3 is adsorbed by F, a typical hole contributor, the MAE also increases drastically, although the easy axis maintains out-of-plane. Our study illustrates the promising potential of electrostatic doping induced by charge transfer in tuning the magnetization orientation and enhancing ferromagnetism in monolayer CrI_3.

2. Computational methods

Our density functional theory (DFT) calculations were carried out using Vienna *ab initio* simulation package (VASP) [31] code with the projector augmented-wave (PAW) method [32]. The exchange correlation interaction of electrons was treated within the generalized-gradient approximation (GGA) in the formalism of Perdew-Burke-Ernzerhof (PBE) [33]. The plane-wave cut-off energy was set to be 500 eV. The Brillouin zone was sampled by using a $6 \times 6 \times 1$ Γ-centered Monkhorst–Pack k-point grid for conventional unit cell and $4 \times 4 \times 1$ k-point for $2 \times 2 \times 1$ supercell [34]. In this work, all the atomic structures were fully relaxed until the force on each atom is smaller than 0.01 eV/Å, and the total energy was converged to be within at least 10^{-6} eV (10^{-8} eV for MAE calculations) during electron configuration relaxation. A vacuum space of larger than 20 Å along the out of the plane z axis was employed to avoid the artificial interactions between image layers. Spin-orbit coupling was taken into account to obtain the MAE, which was evaluated based on the total energy difference between in-plane [100] and out-of-plane [001] magnetization direction, namely, $\mathrm{MAE} = E_{[100]} - E_{[001]}$. Therefore, the positive and negative values of MAE denote that the easy magnetization axis is perpendicular and parallel to the plane of monolayer CrI_3, respectively. Convergence test has been carefully carried out for cut-off energy and k-point sampling on MAE. The results show that the values of MAE converge to 10^{-5} eV/Cr as cut-off energy changes from 400 eV to 550 eV, and k mesh from $4 \times 4 \times 1$ to $8 \times 8 \times 1$ for pristine CrI_3. Because of the non-negligible uniaxial magnetic anisotropy, Heisenberg model including single ion anisotropy is used to describe the magnetic behavior. The Curie-temperature (T_c) of CrI_3 monolayer was then estimated by using Monte Carlo (MC) simulation based on the Heisenberg model [35].

$$H = -J_1 \sum_{i,j} S_i \cdot S_j - J_2 \sum_{i,l} S_i \cdot S_l - A(S_i^z)^2, \quad (1)$$

where J_1 and J_2 are the first and second nearest neighboring exchange parameters, respectively. S_i is the spin vector of each atom, S_i^z is the spin component along the z direction, and A is anisotropy energy parameter. To extract the J_1 and J_2, we considered three different magnetic configurations as shown in Fig. 1. We fit the total energies obtained from DFT calculations to the Heisenberg spin Hamiltonian defined on a honeycomb lattice. Here, $|S| = 3/2$. Using these DFT derived magnetic exchange parameters, the Curie temperature is then estimated using MC simulations with VAMPIRE software package [36].

3. Results and discussion

3.1. Electronic structure and magnetic properties of pristine monolayer CrI_3

First, we investigated the structure, magnetism, and MAE of the pristine monolayer CrI_3 in a $2 \times 2 \times 1$ supercell as shown in Fig. 1(a). The pristine monolayer CrI_3 belongs to the $P\bar{3}1m$ space group. It consists of 2D honeycomb network of Cr atoms, which are sandwiched between two atomic planes of I. Moreover, Cr atoms are coordinated by edge-sharing octahedra with six I atoms. Our calculation indicates that the most stable magnetic state is the FM state among all the considered magnetic configurations [Fig. 1(b)]. The studied AFM1 and AFM2 are unfavored in energy by 37 and 22 meV per unit cell than the FM configuration, respectively. For the FM ground state, the optimized lattice constant is 7.006 Å, and the Cr-I bond length is 2.738 Å. These results are in good agreement with earlier reports [37]. As shown in Fig. 1(c), the monolayer CrI_3 is semiconductor with a band gap of 1.18 eV, in line with earlier experimental and the theoretical results of 1.2 eV [15] and 1.124 eV [38] respectively. The valence band maximum (VBM) is dominated by the hybrid orbitals of Cr-d and I-p, while the conduction band minimum (CBM) is dominated by the Cr-d orbital. The calculated MAE is about 0.990 meV/Cr, which is consistent with earlier theoretical results, 0.980 meV/Cr [39] and 0.840 meV/Cr [37]. The positive value indicates an out-of-plane easy magnetization axis.

3.2. Effect of electrostatic doping on MAE

As is well known, MAE is an important parameter to characterize FM materials besides the magnetization and T_C. Previous work indicated that magnetic properties of CrI_3 monolayer are sensitive to electrostatic doping [27]. An interesting question is whether the MAE is tunable by charge doping, which can be easily realized

by surface adsorption. We calculated the MAE with charge doping by only adding electrons or holes to pristine monolayer CrI_3 (cf. Fig. 2). Clearly, the MAE can be largely tuned by charge doping, show little oscillation within the investigated charge range. The system has a magnetic phase transition from the out-of-plane to the in-plane easy-axis after exceeding certain electron doping (~ -0.085 e/u.c.). While for the hole doping, the easy axis remains out-of-plane when the doping is less than a certain concentration (~ 0.852 e/u.c.), and changes from out-of-plane to in-plane when larger than the certain doping concentration.

After studying the hypothetical doping monolayer CrI_3 system, we turn to the realistic charge doping by adsorption in the following subsections. Here we choose Li (F) atoms as electron (hole) donors in our studies, and study the effect of adsorption on the electronic structure and magnetic properties of monolayer CrI_3.

3.3. Li adsorption

To obtain the most energetically favorable adsorption configuration, we have considered three adsorption sites labeled as (I) hollow (at the hollow of honeycomb network of Cr atoms), (II) Cr-top (at the top of Cr atom), and (III) I-top (at the top of I atom) with one Li atom adsorption on the surface of monolayer CrI_3 in $2 \times 2 \times 1$ supercell, in which the Li adsorption coverage is 3.125%, as shown in Fig. 3(a). After fully relaxation, the I-top configuration is found to relax into the hollow site spontaneously. As listed in Table 1, the hollow site configuration has the lowest energy, and the Cr-top configuration is the most unfavored. The similar results were also obtained in a conventional unit cell of CrI_3, which contains 9 atoms with 12.5% Li coverage. For the case of the hollow site, the Li atom is located at the center of honeycomb network composed of Cr atoms. The adsorption energy of Li at the hollow site is calculated to be -3.109 eV, indicating that Li atoms will not be clustering as the cohesive energy is around 1.605 eV. Hence the hollow site configuration is considered as the most stable configuration, and will be focused in the following sections.

From the top view of a fully relaxed hollow site configuration with 12.5% coverage, the Li atom is located in the middle of the hollow site surrounded by six I atoms. The lattice constant of CrI_3-Li unit cell is slightly elongated to 7.094 Å. The Cr-I bond length (2.805 Å) is obviously longer than that of the pristine one (2.738 Å) accordingly. Meanwhile, the distance between Li and nearest I atom is about 2.952 Å. These changes of local structure will influence the electronic structure. As illustrated in Fig. 3(b), the Li-*s* and I-*p* orbitals are coupled, indirectly altering the hybridization between I-*p* and Cr-*d* orbitals. Comparing Fig. 1(c) with 3(b), we find that the Fermi level is pushed up and cross the spin-polarized conduction bands in CrI_3-Li. As expected, Li atoms provide electrons to monolayer CrI_3, leading to half-metallic character of CrI_3-Li, i.e. the spin-up channel are metallic, while spin-down sub-band remains a sizable bandgap of 2.66 eV as shown in Fig. 3(c). Furthermore, the charge distribution in CrI_3-Li system is remarkably different from the pristine one based on Bader analysis, as listed in Table 2. Obviously, each Li transfer 0.887 e to the surrounding I atoms in CrI_3-Li. The Li-I charge transfer indirectly results in Li atoms donating par-

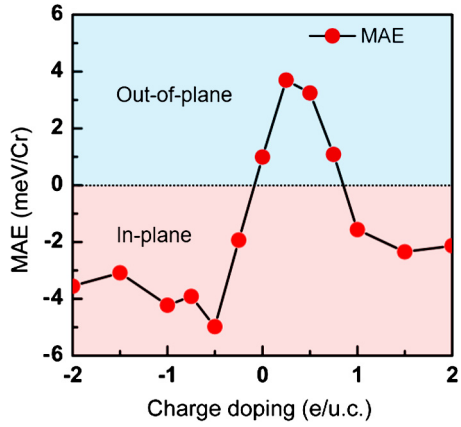

Fig. 2. The MAE of monolayer CrI_3 with different Charge doping. The zero doping indicates the pristine system without charge doping. The negative and positive charge doping represent electron and hole doping, respectively.

Table 1
The calculated adsorption energies (E_a) per supercell of Li on CrI_3 at the coverage of 3.125%. The I-top configuration of CrI_3-Li is relaxed to the hollow structure spontaneously in the simulation.

Configuration	Hollow	Cr-top	I-top
E_a (eV)	−3.109	−2.328	–

Table 2
Charge transfer based on Bader charge calculation in CrI_3 and CrI_3-Li unit cell, respectively. A negative value indicates charge accumulation on the respective atom, while a positive value indicates charge depletion.

	CrI_3		CrI_3-Li		
Atom	Cr	I	Cr	I	Li
Charge transfer	1.015	−0.338	1.002	−0.482	0.887

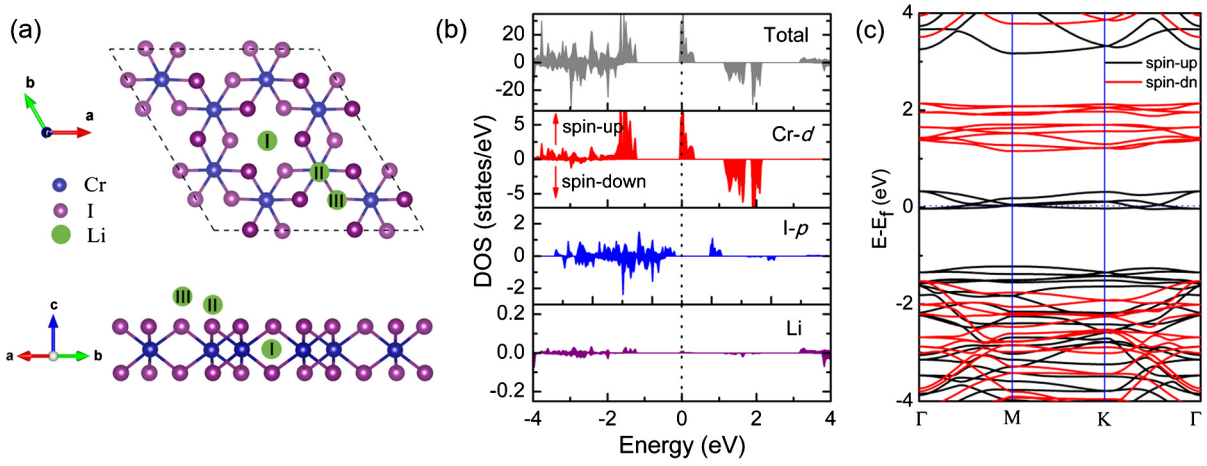

Fig. 3. (a) Top view and side view for crystalline structures of three adsorption configurations of CrI_3-Li in $2 \times 2 \times 1$ supercell with 3.125% Li adsorption coverage. I) hollow, II) Cr-top, III) I-top. Blue, purple and green spheres represent Cr, I, and Li atoms, respectively. Spin-resolved total and partial density of states (b), and band structure (c) for monolayer CrI_3 covered with 12.5% Li. The Fermi level is set to zero as marked with the dot line.

tial electrons to Cr atoms, which brings about an electron doping effect. These results indicate that charge transfer due to Li adsorption can significantly affect the electronic properties of CrI_3.

Consequently, we investigated the effects of Li adsorption on the magnetic properties of CrI_3. The total energy difference between the most stable AFM and FM configuration ΔE is 51.4 meV per unit cell, which is higher than that of the pristine one by 22.5 meV, indicating the FM coupling in CrI_3-Li is enhanced by Li adsorption. It is clear that the total magnetic moment is mainly contributed by Cr atoms, with 3.46 μ_B for each Cr^{3+}, much higher than that of the pristine one ($\sim 3.10\ \mu_B$). The enhancement of the magnetic moment from Cr ions as Li adsorption can be understood by a simple picture (cf. Fig. 4). In an octahedral coordination, the d orbitals of Cr^{3+} split into triply degenerated t_{2g} (d_{xy}, d_{yz} and d_{xz}) and doubly degenerated e_g (d_{z^2} and $d_{x^2-y^2}$), the former with lower energy. In pristine CrI_3, each octahedrally coordinated Cr^{3+} has a $3d^3$ configuration, and the three t_{2g} orbitals are singly occupied with parallel spin (Fig. 4a). Whereas in CrI_3-Li, due to an electron doping effect, besides three electrons occupy the three t_{2g} orbitals, the other electrons occupy the higher e_g orbital according to Hund's rules (Fig. 4b), thus resulting in larger magnetic moment. In addition, the iso-surface of the spin density ($\rho_\uparrow - \rho_\downarrow$) for CrI_3 and CrI_3-Li are plotted in Fig. 4(c) and 4(d), indicating that the Cr atoms are more spin-polarized, while I atoms are slightly antiferromagnetically polarized in CrI_3-Li than that in pristine CrI_3. These results further confirm that the ferromagnetism can be enhanced after Li adsorption.

The impact of Li coverage on the electronic and magnetic properties of monolayer CrI_3 is also investigated. When Li coverage changes from 0% to 12.5%, it is found that the FM configurations are always energetically favored. In fact, the ferromagnetism is almost linearly enhanced as the Li coverage increases, along with the local spin moment of the Cr [cf. Fig. 5(a)]. Moreover, the energy difference ΔE is two times greater than that of pristine one at the coverage of 12.5%. These results indicate that the charge transfer can improve the magnetic stability while maintain half-metallicity under all considered coverages.

One can also observe how MAE changes with Li coverage as shown in Fig. 5(b). When Li is adsorbed onto monolayer CrI_3, the MAE values change from positive to negative at certain coverage (between 3% and 6%) and increase negatively and monotonically with increasing Li adsorption coverage. For example, the MAE changes from 0.990 meV/Cr to −5.785 meV/Cr while Li adsorption coverage increases from 0% to 12.5%. The change of MAE is quite similar to that of pure electron doping, verifying our expectation. These results clearly show that we can effectively switch the easy magnetization orientation from out-of-plane to the in-plane direction by adsorbing Li atoms. We attribute the change of MAE to the electron doping effect induced by charge transfer between Li and Cr atoms. It should be noted that there is almost no difference in energy with respect to the different in-plane directions from our DEF calculations. For example, the total energy difference between in-plane [100], [010], [110] and out-of-plane [001] magnetization direction are −5.785, −5.903 and −5.996 meV/Cr. In fact, a similar conclusion was also reported by Webster et al. [37].

As mentioned above, all the considered CrI_3-Li monolayer prefer FM coupling. It is important to evaluate the T_C affected by Li adsorption, for future application of spintronic devices. Based on the Heisenberg model, the T_c can be estimated by using MC simulations. For the pristine CrI_3, our calculated exchange parameters J_1 and J_2 are 2.755 meV and 0.559 meV, and T_C is estimated to be around 65 K correspondingly. This is slightly overestimated compared with the experimental measurement of 45 K for the monolayer CrI_3 [19], but is approximately equal to the experimental values for the bulk CrI_3 [15]. The magnetic moments of Cr ions increase monotonically, up to 3.46 μ_B when Li coverage reaches 12.5%. This would enhance the magnetic coupling between Cr atoms, and consequently resulting in larger exchange energy and higher Curie temperature. For example, the exchange parameter J_1 are 3.832 meV, 4.951 meV, 5.821 meV, 6.581 meV, and J_2 are 0.438 meV, 0.815 meV, 0.838 meV, 1.208 meV, when Li coverage is 3.125%, 6.25%, 9.375% and 12.5% in CrI_3-Li systems, respectively. The T_C increases with the increasement of Li adsorption coverage, as shown in Fig. 5(c). Although the T_C may be overestimated, it should be noted that the increasement trend of monolayer CrI_3 with Li adsorption. The higher T_C indicate that the CrI_3 monolayer with electron doping may be a promising spintronic material. Moreover, Song et al. [26] reported that the MAE of monolayer $Cr_2Ge_2Te_6$ can be enhanced by H and alkali-metal adsorption,leading to a significant increase of and Curie temperature. Liu et al. [40] reported that the Curie temperature and MAE of lay-

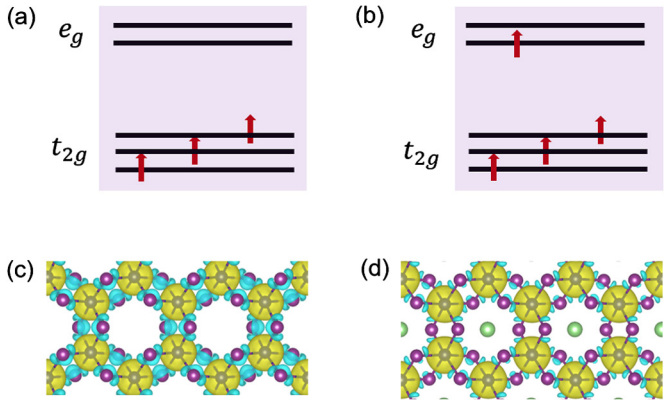

Fig. 4. Schematic diagrams of Cr^{3+} d orbitals in (a) pristine CrI_3 and (b) CrI_3-Li. Iso-surface of spin density of (a) pristine CrI_3 and (b) CrI_3-Li with a value of 0.003 e/Å^3. Yellow and blue represent majority and minority spin channels, respectively.

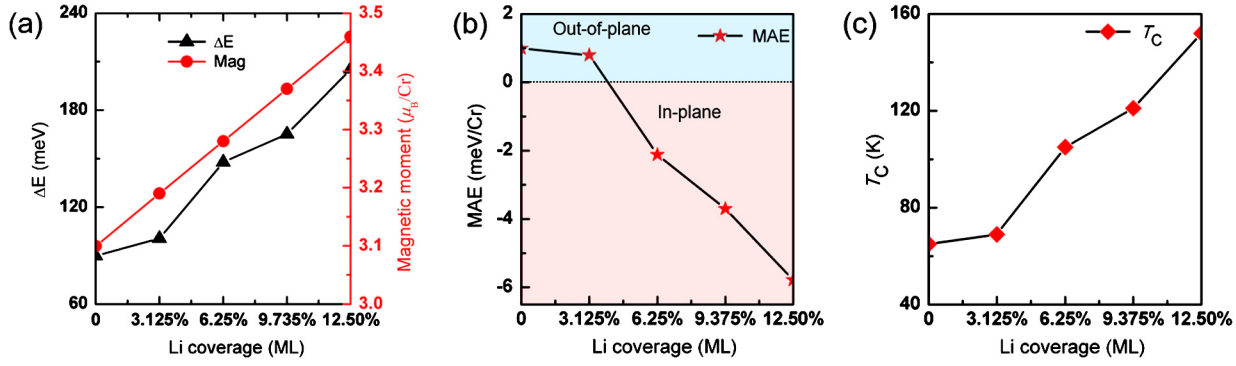

Fig. 5. (a) The local magnetic moment of Cr and total energy differences ΔE between the most stable AFM states and FM states, (b) magnetic anisotropy energy as well as (c) Curie temperature T_C of CrI_3-Li in $2 \times 2 \times 1$ supercell with different Li adsorption coverage.

ered Bi_2O_2Se can be largely enhanced by transition metal atoms doping. Ma et al. [41] reported that the MAE of CrX (X = P, As) monolayer can be enhanced by electron and hole doping. Comparing these systems, one can learn that charge doping likely to enhance the exchange interactions, MAE, as well as improve the Curie temperature of two dimensional magnetic systems.

3.4. F adsorption

The adsorption of F atoms on monolayer CrI_3 is considered to simulate the practical hole doping. Since the electronegativity of F is stronger than I, direct charge transfer may occur between F and Cr, thus leading to hole doping. To confirm the most stable adsorption configuration, we also considered three initial adsorption configurations as mentioned above. It is found that F atoms always relax far away from the initial high symmetrical sites. For example, in the case of the hollow site configuration, the distance between Cr and nearest I is about 2.726 Å, which is obviously shorter than that of CrI_3-Li (2.805 Å). Meanwhile, the bond length of F-Cr1 and F-Cr2 are 4.896 Å and 3.874 Å. The distance between F and nearest I atom is about 2.083 Å, much shorter than that of Li-I (2.952 Å) in CrI_3-Li. These results indicate that the F atoms are relaxed far away from the hollow site and the structure is remarkably distorted.

In order to qualitatively reveal the effect of the hole doping and compare with CrI_3-Li, the MAE of CrI_3-F was also calculated with F atoms fixed at the hollow site as in CrI_3-Li. In contrast to that of CrI_3-Li, F adsorption significantly enhances the MAE, but is not able to alter the magnetic orientation. For example, the MAE of CrI_3-F is as large as 3.925 meV/Cr and 7.070 meV/Cr when F coverage is 3.125% and 12.5% respectively. Such a difference can be well expected from the electronegativity of Li and F atom. These results agree well with those obtained by pure charge doping as described above, showing that electrostatic doping induced by surface adsorption could tune the MAE of monolayer CrI_3. Especially, electron doping can drastically tune the spin orientations. Therefore, the strong coupling between charge transfer and MAE provides an effective way to control spin orientation, which provides a very promising means for the application of spin electronics devices in the future.

4. Conclusions

In summary, the electronic and magnetic properties of monolayer CrI_3 could be tuned by the surface adsorption. Our results show that the monolayer CrI_3 can be switched from semiconductor to half-metal, and the magnetic moments on Cr and T_C can be largely enhanced by Li adsorption. Interestingly, the CrI_3-Li exhibits robust magnetic anisotropy (-5.785 meV/Cr) with an in-plane easy magnetization axis, almost 6 times compared with that of the pristine CrI_3 (0.990 meV/Cr) with an out-of-plane easy axis. Moreover, the value of MAE increases linearly with the increasement of the Li adsorption coverage. On the contrary, F adsorption preserves the easy magnetization axis out-of-plane, and leads to a larger increase of MAE (7.070 meV/Cr). The robust MAE together with the enhanced ferromagnetism of monolayer CrI_3 induced by surface adsorption may provide promising applications in 2D spintronic devices.

CRediT authorship contribution statement

Qin-Fang Xu: Conceptualization, Data curation, Funding acquisition, Investigation, Methodology, Visualization, Writing - original draft, Writing - review & editing. **Wen-Qiang Xie:** Formal analysis. **Zhi-Wei Lu:** Formal analysis. **Yu-Jun Zhao:** Funding acquisition, Supervision, Writing - review & editing.

Declaration of competing interest

The authors declare that they have no known competing financial interests or personal relationships that could have appeared to influence the work reported in this paper.

Acknowledgements

This work was supported by NSFC (Grant No. 11574088), the Innovative and Strong School Project of Guangzhou Maritime University (2014E073, G410304, F410102), and Innovation and Start-up Business Education Project of Universities in Guangzhou (2019PT201).

References

[1] L. Tao, E. Cinquanta, D. Chiappe, C. Grazianetti, M. Fanciulli, M. Dubey, A. Molle, D. Akinwande, Nat. Nanotechnol. 10 (2015) 227.
[2] M. Ghorbani-Asl, A. Kuc, P. Miró, T. Heine, Adv. Mater. 28 (2016) 853.
[3] L. Li, Y. Yu, G.J. Ye, Q. Ge, X. Ou, H. Wu, D. Feng, X.H. Chen, Y. Zhang, Nat. Nanotechnol. 9 (2014) 372.
[4] S. Albarakati, C. Tan, Z.-J. Chen, J.G. Partridge, G. Zheng, L. Farrar, E.L.H. Mayes, M.R. Field, C. Lee, Y. Wang, Y. Xiong, M. Tian, F. Xiang, A.R. Hamilton, O.A. Tretiakov, D. Culcer, Y.-J. Zhao, L. Wang, Sci. Adv. 5 (2019) eaaw0409.
[5] S. Chen, G. Shi, Adv. Mater. 29 (2017) 1605448.
[6] X. Zhou, J. Zhou, Y. Yu, J. Ma, X. Sun, L. Hu, NANO 12 (2017) 1750121.
[7] M. Osada, S. Yoguchi, M. Itose, B.-W. Li, Y. Ebina, K. Fukuda, Y. Kotani, K. Ono, S. Ueda, T. Sasaki, Nanoscale 6 (2014) 14227.
[8] S. Dutta, A.K. Manna, S.K. Pati, Phys. Rev. Lett. 102 (2009) 096601.
[9] O.V. Yazyev, L. Helm, Phys. Rev. B 75 (2007).
[10] P.A. Khomyakov, G. Giovannetti, P.C. Rusu, G. Brocks, J. van den Brink, P.J. Kelly, Phys. Rev. B 79 (2009).
[11] S. Lebègue, T. Björkman, M. Klintenberg, R.M. Nieminen, O. Eriksson, Phys. Rev. X 3 (2013).
[12] A.A. Balandin, S. Ghosh, W. Bao, I. Calizo, D. Teweldebrhan, F. Miao, C.N. Lau, Nano Lett. 8 (2008) 902.
[13] H. Kumar, N.C. Frey, L. Dong, B. Anasori, Y. Gogotsi, V.B. Shenoy, ACS Nano 11 (2017) 7648.
[14] Y. Sun, Z. Zhuo, X. Wu, J. Yang, Nano Lett. 17 (2017) 2771.
[15] M.A. McGuire, H. Dixit, V.R. Cooper, B.C. Sales, Chem. Mater. 27 (2015) 612.
[16] L. Dong, H. Kumar, B. Anasori, Y. Gogotsi, V.B. Shenoy, J. Phys. Chem. Lett. 8 (2017) 422.
[17] F. Wu, C. Huang, H. Wu, C. Lee, K. Deng, E. Kan, P. Jena, Nano Lett. 15 (2015) 8277.
[18] C. Gong, L. Li, Z. Li, H. Ji, A. Stern, Y. Xia, T. Cao, W. Bao, C. Wang, Y. Wang, Z.Q. Qiu, R.J. Cava, S.G. Louie, J. Xia, X. Zhang, Nature 546 (2017) 265.
[19] B. Huang, G. Clark, E. Navarro-Moratalla, D.R. Klein, R. Cheng, K.L. Seyler, D. Zhong, E. Schmidgall, M.A. McGuire, D.H. Cobden, W. Yao, D. Xiao, P. Jarillo-Herrero, X. Xu, Nature 546 (2017) 270.
[20] M. Bonilla, S. Kolekar, Y. Ma, H.C. Diaz, V. Kalappattil, R. Das, T. Eggers, H.R. Gutierrez, M.-H. Phan, M. Batzill, Nat. Nanotechnol. 13 (2018) 289.
[21] D.J. O'Hara, T. Zhu, A.H. Trout, A.S. Ahmed, Y.K. Luo, C.H. Lee, M.R. Brenner, S. Rajan, J.A. Gupta, D.W. McComb, R.K. Kawakami, Nano Lett. 18 (2018) 3125.
[22] Y. Deng, Y. Yu, Y. Song, J. Zhang, N.Z. Wang, Z. Sun, Y. Yi, Y.Z. Wu, S. Wu, J. Zhu, J. Wang, X.H. Chen, Y. Zhang, Nature 563 (2018) 94.
[23] A.F. May, D. Ovchinnikov, Q. Zheng, R. Hermann, S. Calder, B. Huang, Z. Fei, Y. Liu, X. Xu, M.A. McGuire, ACS Nano 13 (2019) 4436.
[24] N.D. Mermin, H. Wagner, Phys. Rev. Lett. 17 (1966) 1307.
[25] D.R. Klein, D. MacNeill, J.L. Lado, D. Soriano, E. Navarro-Moratalla, K. Watanabe, T. Taniguchi, S. Manni, P. Canfield, J. Fernández-Rossier, P. Jarillo-Herrero, Science 360 (2018) 1218.
[26] C. Song, W. Xiao, L. Li, Y. Lu, P. Jiang, C. Li, A. Chen, Z. Zhong, Phys. Rev. B 99 (2019) 214435.
[27] S. Jiang, L. Li, Z. Wang, K.F. Mak, J. Shan, Nat. Nanotechnol. 13 (2018) 549.
[28] N. Richter, D. Weber, F. Martin, N. Singh, U. Schwingenschlögl, B.V. Lotsch, M. Kläui, Phys. Rev. Mater. 2 (2018) 024004.
[29] Y. Liu, L. Wu, X. Tong, J. Li, J. Tao, Y. Zhu, C. Petrovic, Sci. Rep. 9 (2019) 13599.
[30] Y. Liu, C. Petrovic, Phys. Rev. B 97 (2018) 174418.
[31] G. Kresse, J. Furthmüller, Phys. Rev. B 54 (1996) 11169.
[32] P.E. Blöchl, Phys. Rev. B 50 (1994) 17953.
[33] J.P. Perdew, K. Burke, M. Ernzerhof, Phys. Rev. Lett. 77 (1996) 3865.
[34] H.J. Monkhorst, J.D. Pack, Phys. Rev. B 13 (1976) 5188.
[35] B. Wang, Q. Wu, Y. Zhang, Y. Guo, X. Zhang, Q. Zhou, S. Dong, J. Wang, Nanoscale Horiz. 3 (2018) 551.

[36] R.F.L. Evans, W.J. Fan, P. Chureemart, T.A. Ostler, M.O.A. Ellis, R.W. Chantrell, J. Phys. Condens. Matter 26 (2014) 103202.
[37] L. Webster, J. Yan, Phys. Rev. B 98 (2018) 144411.
[38] Z. Wu, J. Yu, S. Yuan, Phys. Chem. Chem. Phys. 21 (2019) 7750.
[39] P. Jiang, L. Li, Z. Liao, Y.X. Zhao, Z. Zhong, Nano Lett. 18 (2018) 3844.
[40] X. Liu, D. Legut, R. Zhang, T. Wang, Y. Fan, Q. Zhang, Phys. Rev. B 100 (2019) 054438.
[41] A. Ma, P. Wang, C. Zhang, Nanoscale (2018), https://doi.org/10.1039/C9NR10322H.